A comparative study of penalty formulations in elasticity

Adair R. Aguiar
Department of Structural Engineering, EESC/USP, São Carlos, SP – Brazil

Abstract

A.R. Aguiar (2004, 2006) [1, 2] have considered a class of two-dimensional problems in classical linear elasticity for which material overlapping occurs. Of course, material overlapping is not physically realistic, and one possible way to prevent it uses a constrained minimization theory. In this theory, a minimization problem consists of minimizing the total potential energy of a linear elastic body subject to the constraint that the deformation field be locally invertible. A.R. Aguiar (2004, 2006) [1, 2] have used, respectively, an interior and an exterior penalty formulation of the minimization problem together with a standard finite element method to compute the minimizers. The formulation consists of finding the displacement field that minimizes an augmented potential energy functional, which is composed of the potential energy of linear elasticity theory and of a penalty functional divided by a penalty parameter. In the interior penalty formulation, the penalty functional becomes unbounded as we approach the boundary of the set of all kinematically admissible deformation fields from inside the set. A sequence of minimizers belonging to this set and parameterized by the penalty parameter is then constructed. As the penalty parameter becomes unbounded, the sequence is shown to converge to the solution of the original constrained minimization problem. In the exterior penalty formulation, the penalty functional is bounded everywhere and is zero inside the set of kinematically admissible fields. A sequence of minimizers, parameterized by the penalty parameter, is also constructed and is shown to converge to the solution of the original constrained minimization problem as the penalty parameter goes to zero. In this work, we compare both formulations by solving a singular problem in plane elasticity. In particular, we determine the convergence ratio in both cases and show numerical results which indicate that, for a fixed finite element mesh, the sequence of numerical solutions obtained with the exterior penalty formulation converges faster than the sequence of numerical solutions obtained with the interior penalty formulation.

Keywords: anisotropic elasticity, singularity, constrained optimization, penalty method, Finite Element Method.

1 Introduction

There are problems in the classical linear theory of elasticity whose closed form solutions, while satisfying the governing equations of equilibrium together with well-posed boundary conditions, allow

Mechanics of Solids in Brazil 2007, Marcílio Alves & H.S. da Costa Mattos (Editors)
Brazilian Society of Mechanical Sciences and Engineering, ISBN 978-85-85769-30-7

material overlapping to occur. Typically, problems of this kind involve some sort of singularity, and strains exceeding level acceptable from the point of view of a linear theory occur around the singular points.

References [1, 2] have considered a two-dimensional problem in classical linear elasticity for which material overlapping occurs. The problem, presented in [3], concerns the equilibrium of a circular homogeneous disk, which is radially compressed along its external contour by a uniformly distributed normal force. The requirement that the displacement field be rotationally symmetric with respect to the center of the disk allows the derivation of a closed form solution that predicts overlapping of material in a certain region occupied by the linear elastic disk.

One possible way to prevent the anomalous behavior of self-intersection is proposed by [4]. It combines the linear theory with the imposition of local injectivity constraint through a Lagrange multiplier technique. These authors investigate the problem of minimizing the total potential energy $\mathcal{E}$ of classical linear elasticity on an admissible set $\mathcal{A}_\varepsilon$ of vector-valued functions $\mathbf{v}$ that satisfy the injectivity constraint $\det(\mathbf{1} + \nabla \mathbf{v}) \geq \varepsilon > 0$ for a sufficiently small $\varepsilon \in \mathbb{R}$. In particular, they show the existence of a solution for the constrained minimization problem in two dimensions. The constrained problem is, however, highly nonlinear and, in general, needs to be solved numerically.

References [1, 2, 5] present Finite Element approaches to solve this class of constrained problems. In the Obeidat's approach, a carefully designed algorithm is required to keep track of all subdomains of the reference configuration where the injectivity constraint is violated.

Our approach in [1] is based on an *interior penalty formulation*, which consists of replacing $\mathcal{E}$ by a penalized functional $\mathcal{E}_\gamma = \mathcal{E} + \mathcal{Q}/\gamma$, where γ is an arbitrary positive number and $\mathcal{Q}$ is a penalty functional defined on the constraint set $\mathcal{A}_\varepsilon$. The penalty functional is non-negative on $\mathcal{A}_\varepsilon$, satisfies $\mathcal{Q}[\mathbf{v}] \to \infty$ as $\mathbf{v}$ approaches the boundary of $\mathcal{A}_\varepsilon$, and is designed so that minimizers of $\mathcal{E}_\gamma[\cdot]$ lie in the interior of the constraint set $\mathcal{A}_\varepsilon$; hence the term *interior penalty method*. Thus, the penalty formulation of the constrained problem consists of finding $\mathbf{u}_\gamma \in \mathcal{A}_\varepsilon$ that minimizes the penalized functional $\mathcal{E}_\gamma$ over the constraint set $\mathcal{A}_\varepsilon$.

Another approach considered by [2] is based on an *exterior penalty formulation*, which consists of replacing $\mathcal{E}$ by a penalized functional $\mathcal{E}_\delta = \mathcal{E} + \mathcal{P}/\delta$, where δ is an arbitrary positive number and $\mathcal{P}$ is a penalty functional defined on the whole set $\mathcal{A}$. The penalty functional is non-negative on $\mathcal{A}$ and vanishes on $\mathcal{A}_\varepsilon$. In general, the minimizers of $\mathcal{E}_\delta[\cdot]$ lie in the exterior of the constraint set $\mathcal{A}_\varepsilon$; hence the term *exterior penalty method*. Thus, the penalty formulation of the constrained problem consists of finding $\mathbf{u}_\delta \in \mathcal{A}$ that minimizes the penalized functional $\mathcal{E}_\delta$ over the set $\mathcal{A}$. This method has the advantage of yielding an unconstrained minimization problem.

In Section 2 we apply both penalty formulations on the class of constrained minimization problems considered by [4]. In Section 3 we review some results presented by these authors concerning the compressed disk problem in the context of both the unconstrained and the constrained theories. In Section 4 we use the Finite Element Method to obtain discrete problems from the penalty formulations of the constrained disk problem and discuss briefly a strategy presented by [6] to solve this class of problems. The resulting numerical scheme is simple to implement, converges much faster than previous schemes presented by [1, 2], and can be applied in the numerical solution of problems in any dimension. In Section 5 we compare the numerical results obtained from the solutions of the discrete problems

Mechanics of Solids in Brazil 2007, Marcílio Alves & H.S. da Costa Mattos (Editors)
Brazilian Society of Mechanical Sciences and Engineering, ISBN 978-85-85769-30-7

with analytical results obtained from the closed form solution of the constrained minimization problem considered in Section 3. In Section 6 we present some concluding remarks.

2 The penalty functional formulation

Let $\mathcal{B} \subset \mathbb{R}^2$ be the undistorted natural reference configuration of a body. Points $\mathbf{x} \in \mathcal{B}$ are mapped to points $\hat{\mathbf{x}} = \mathbf{f}(\mathbf{x}) \equiv \mathbf{x} + \mathbf{u}(\mathbf{x}) \in \mathbb{R}^2$, where $\mathbf{u}(\mathbf{x})$ is the displacement of $\mathbf{x}$. The boundary $\partial\mathcal{B}$ of $\mathcal{B}$ is composed of two non-intersecting parts, $\partial_1\mathcal{B}$ and $\partial_2\mathcal{B}$, $\partial_1\mathcal{B} \cup \partial_2\mathcal{B} = \partial\mathcal{B}$, $\partial_1\mathcal{B} \cap \partial_2\mathcal{B} = \emptyset$, such that $\mathbf{u}(\mathbf{x}) = 0$ for $\mathbf{x} \in \partial_1\mathcal{B}$ and such that a dead load traction field $\bar{\mathbf{t}}(\mathbf{x})$ is prescribed for $\mathbf{x} \in \partial_2\mathcal{B}$. In addition, a body force $\mathbf{b}(\mathbf{x})$ per unit volume of $\mathcal{B}$ acts on points $\mathbf{x} \in \mathcal{B}$.

We consider the problem of minimum potential energy:

$$\min_{\mathbf{v}\in\mathcal{A}_\varepsilon} \mathcal{E}[\mathbf{v}]\,, \qquad \mathcal{E}[\mathbf{v}] \equiv \frac{1}{2}\, a[\mathbf{v},\mathbf{v}] - f[\mathbf{v}]\,, \tag{1}$$

where

$$a[\mathbf{v},\mathbf{v}] \equiv \int_{\mathcal{B}} \mathbb{C}[\mathbf{E}]\cdot\mathbf{E}\, d\mathbf{x}\,, \qquad f[\mathbf{v}] \equiv \int_{\mathcal{B}} \mathbf{b}\cdot\mathbf{v}\, d\mathbf{x} + \int_{\partial_2\mathcal{B}} \bar{\mathbf{t}}\cdot\mathbf{v}\, d\mathbf{x}\,, \tag{2}$$

and $\mathbf{E} \equiv \left[\nabla\mathbf{v} + (\nabla\mathbf{v})^T\right]/2$ is the infinitesimal strain tensor field. The functional $\mathcal{E}[\cdot]$ is the total potential energy of classical linear theory of elasticity. Furthermore,

$$\mathcal{A}_\varepsilon \equiv \{\mathbf{v} : W^{1,2}(\mathcal{B}) \to \mathbb{R}^2 \big|\, \det(\mathbf{1} + \nabla\mathbf{v}) \geq \varepsilon > 0, \mathbf{v} = \mathbf{0} \text{ a.e. on } \partial_1\mathcal{B}\} \tag{3}$$

is the class of admissible displacement fields and $\mathbb{C} = \mathbb{C}(\mathbf{x})$ is the elasticity tensor, assumed to be positive definite and symmetric. We suppose that $\varepsilon > 0$ in (3) is sufficiently small.

Reference [4] fully characterize the solutions of the minimization problem (1)-(3). In particular, they show that there exists a solution to this problem which does not violate the injectivity constraint $\det(\mathbf{1} + \nabla\mathbf{v}) \geq \varepsilon > 0$ and derive first variation conditions for a minimizer $\mathbf{u} \in \mathcal{A}_\varepsilon$ of $\mathcal{E}[\cdot]$.

Let

$$\mathcal{A} \equiv \{\mathbf{v} : W^{1,2}(\mathcal{B}) \to \mathbb{R}^2 \big|\, \mathbf{v} = \mathbf{0} \text{ a.e. on } \partial_1\mathcal{B}\}\,. \tag{4}$$

We then obtain the first variation of $\mathcal{E}[\cdot]$ at $\mathbf{u}$ in the form $< D\mathcal{E}[\mathbf{u}], \mathbf{v} > \equiv a[\mathbf{u},\mathbf{v}] - f[\mathbf{v}]\,, \forall\, \mathbf{v} \in \mathcal{A}$, where $a[\cdot,\cdot]$ and $f[\cdot]$ are defined in (2). On the other hand, it can be shown that there exists a scalar Lagrange multiplier field $\lambda : \mathcal{L}^2(\mathcal{B}) \to \mathbb{R}$ such that the first variation has the equivalent representation $< D\mathcal{E}[\mathbf{u}], \mathbf{v} > = \int_{\mathcal{B}} \lambda\, \mathrm{cof}\,\nabla\mathbf{f}\cdot\nabla\mathbf{v}\, d\mathbf{x}\,, \forall\, \mathbf{v} \in \mathcal{A}$, where $\mathrm{cof}\,\nabla\mathbf{f}$ is the cofactor of the deformation gradient and we recall from above that $\mathbf{f}(\mathbf{x}) = \mathbf{x} + \mathbf{u}(\mathbf{x})$.

Defining

$$\mathcal{B}_> \equiv \mathrm{int}[\{\mathbf{x} \in \mathcal{B} : \det\nabla\mathbf{f} > \varepsilon\}]\,, \qquad \mathcal{B}_= \equiv \mathrm{int}[\{\mathbf{x} \in \mathcal{B} : \det\nabla\mathbf{f} = \varepsilon\}]\,, \tag{5}$$

where $\mathrm{int}[\cdot]$ denotes the interior of a set, the necessary first variation conditions for the existence of a minimizer are given by

- The Euler-Lagrange equations

$$\mathrm{Div}\,\mathbf{T} + \mathbf{b} = \mathbf{0} \quad \text{in } \mathcal{B}_> \,, \quad \mathrm{Div}(\mathbf{T} - \varepsilon\lambda(\nabla\mathbf{f})^{-T}) + \mathbf{b} = \mathbf{0} \,, \quad \lambda \geq 0 \,, \quad \text{in } \mathcal{B}_= \,, \tag{6}$$

  together with the boundary conditions

$$\mathbf{T}\,\mathbf{n} = \bar{\mathbf{t}} \quad \text{on } \partial\mathcal{B}_> \cap \partial_{\mathbf{2}}\mathcal{B} \,, \quad (\mathbf{T} - \varepsilon\lambda(\nabla\mathbf{f})^{-\mathbf{T}})\,\mathbf{n} = \bar{\mathbf{t}} \quad \text{on } \partial\mathcal{B}_= \cap \partial_{\mathbf{2}}\mathcal{B} \,, \tag{7}$$

  where $\mathbf{T}$ is the stress tensor and $\mathbf{n}$ is a unit normal to $\partial_2\mathcal{B}$.
- Jump conditions across $\Sigma \equiv \bar{\mathcal{B}}_> \cap \bar{\mathcal{B}}_=$, which is assumed to be sufficiently smooth:

$$(\mathbf{T} - \varepsilon\lambda(\nabla\mathbf{f})^{-T})\big|_{\Sigma\cap\bar{\mathcal{B}}_=}\,\mathbf{n} = \mathbf{T}\big|_{\Sigma\cap\bar{\mathcal{B}}_>}\,\mathbf{n} \,, \tag{8}$$

  where $\mathbf{n}$ is a unit normal to Σ and where $\Sigma \cap \bar{\mathcal{B}}_=$ and $\Sigma \cap \bar{\mathcal{B}}_>$ mean that the evaluations are understood as limits to the dividing interface Σ from within $\mathcal{B}_=$ and $\mathcal{B}_>$, respectively.

An *interior penalty functional formulation* of the minimization problem (1)-(3) consists of replacing the energy functional (1.b) by a penalized potential energy functional $\mathcal{E}_\gamma : \mathcal{A}_\varepsilon \to \bar{\mathbb{R}}$, $\bar{\mathbb{R}} \equiv \mathbb{R} \cup \{\infty\}$, of the form

$$\mathcal{E}_\gamma[\mathbf{u}] = \mathcal{E}[\mathbf{u}] + \frac{1}{\gamma}\mathcal{Q}[\mathbf{u}] \,, \tag{9}$$

where $\gamma > 0$ is a penalty parameter and $\mathcal{Q} : \mathcal{A}_\varepsilon \to \bar{\mathbb{R}}$ is an *interior penalty functional*, also called *barrier functional*. The penalty functional is designed so that minimizers of $\mathcal{E}_\gamma[\cdot]$ lie in the interior of the constraint set $\mathcal{A}_\varepsilon$. Thus, the addition of $(1/\gamma)\,\mathcal{Q}$ has the effect of establishing a barrier on the boundary of the constraint set $\mathcal{A}_\varepsilon$ that prevents a search procedure for a minimizer from leaving the set $\mathcal{A}_\varepsilon$. In this work, we consider the *inverse barrier functional*, defined by

$$\mathcal{Q}[\mathbf{v}] = \int_{\mathcal{B}} \frac{1}{\det(\mathbf{1} + \nabla\mathbf{v}) - \varepsilon}\, d\mathbf{x}, \qquad \forall \mathbf{v} \in \mathcal{A}_\varepsilon \,. \tag{10}$$

Observe from (10) that $\mathcal{Q}$ is non-negative on $\mathcal{A}_\varepsilon$ and satisfies $\mathcal{Q}[\mathbf{v}] \to \infty$ as $\mathbf{v}$ approaches the boundary of $\mathcal{A}_\varepsilon$.

The penalty formulation of the minimization problem (1)-(3) consists of finding an admissible displacement field $\mathbf{u}_\gamma \in \mathcal{A}_\varepsilon$ that minimizes the penalized potential $\mathcal{E}_\gamma[\cdot]$, i.e.,

$$\min_{\mathbf{v}\in\mathcal{A}_\varepsilon} \mathcal{E}_\gamma[\mathbf{v}] \,, \tag{11}$$

where $\mathcal{E}_\gamma[\mathbf{v}]$ is given by the expressions (9), (1.b), (2), and (10). This is a constrained problem, and indeed the functional to be minimized is somewhat more complicated than the original energy functional (1.b). The advantage of considering this problem, however, is that we can use numerical procedures commonly employed in the numerical approximation of solutions of unconstrained problems. Thus, although the minimization problem (11) is a constrained problem from the theoretical point of view, from a computational point of view, it is unconstrained.

On the other hand, an *exterior penalty functional formulation* of the minimization problem (1)-(3) consists of replacing the energy functional (1.b) by a penalized potential energy functional $\mathcal{E}_\delta : \mathcal{A} \to \mathbb{R}$ of the form

$$\mathcal{E}_\delta[\mathbf{u}] = \mathcal{E}[\mathbf{u}] + \frac{1}{\delta}\mathcal{P}[\mathbf{u}]\,, \tag{12}$$

where $\delta > 0$ is a penalty parameter and $\mathcal{P} : \mathcal{A} \to \mathbb{R}$ is a *penalty functional*, which is non-negative in $\mathcal{A}$ and is designed so that $\mathcal{P}[\mathbf{v}]$ increases with the distance from $\mathbf{v}$ to the constraint set $\mathcal{A}_\varepsilon$. In this work, we consider

$$\mathcal{P}[\mathbf{v}] = \frac{1}{2}\int_{\mathcal{B}} \left[\max(0, -p(\mathbf{v}))\right]^2 \, d\mathbf{x}\,, \qquad \forall\, \mathbf{v} \in \mathcal{A}\,, \tag{13}$$

where $\max(0, -p) \equiv (-p + |\,p\,|)/2$ and

$$p(\mathbf{v}) = \det(\mathbf{1} + \nabla\mathbf{v}) - \varepsilon\,. \tag{14}$$

Clearly, $\mathcal{P}[\mathbf{v}] = 0$ if the injectivity constraint is satisfied; otherwise, $\mathcal{P}[\mathbf{v}] > 0$. In Section 4 we see that the choice (13) for $\mathcal{P}$ leads to a discrete version of the penalized energy functional $\mathcal{E}_\delta$ that is continuous and differentiable everywhere.

We then want to find an admissible displacement field $\mathbf{u}_\delta \in \mathcal{A}$ that minimizes the penalized potential $\mathcal{E}_\delta[\cdot]$, i.e.,

$$\min_{\mathbf{v}\in\mathcal{A}} \mathcal{E}_\delta[\mathbf{v}]\,, \tag{15}$$

where $\mathcal{E}_\delta[\mathbf{v}]$ is given by the expressions (12), (1.b), (2), (13), and (14). This is an unconstrained problem, which also has the advantage of yielding discrete minimization problems that can be solved by classical unconstrained optimization techniques.

In Section 4 we use both penalty formulations presented above to construct a numerical scheme that is used in Section 5 for the solution of the constrained plane problem presented in Section 3.2.

3 The disk problem

In this section we review the main results obtained from the solution of a plane problem, which will serve as a model problem in our computations, in the context of both the classical linear theory, Section 3.1, and the constrained minimization theory, Section 3.2.

3.1 The unconstrained disk problem

In classical linear elasticity, the disk problem concerns the equilibrium of a circular homogeneous disk of radius ρ_e, which is radially compressed along its external contour by a uniformly distributed

normal force p per unit length. Relative to the usual orthonormal cylindrical basis $(\mathbf{e}_\rho, \mathbf{e}_\theta)$, the stress and strain tensors are given by

$$\mathbf{T} = \sigma_{\rho\,\rho}\,\mathbf{e}_\rho \otimes \mathbf{e}_\rho + \sigma_{\theta\,\theta}\,\mathbf{e}_\theta \otimes \mathbf{e}_\theta + \sigma_{\rho\,\theta}\,(\mathbf{e}_\rho \otimes \mathbf{e}_\theta + \mathbf{e}_\theta \otimes \mathbf{e}_\rho)\,,$$
$$\mathbf{E} = \epsilon_{\rho\,\rho}\,\mathbf{e}_\rho \otimes \mathbf{e}_\rho + \epsilon_{\theta\,\theta}\,\mathbf{e}_\theta \otimes \mathbf{e}_\theta + \epsilon_{\rho\,\theta}\,(\mathbf{e}_\rho \otimes \mathbf{e}_\theta + \mathbf{e}_\theta \otimes \mathbf{e}_\rho)\,, \tag{16}$$

respectively. These tensors are related to each other by the linear constitutive relations

$$\sigma_{\rho\,\rho} = \frac{1}{1-\nu_\rho\nu_\theta}(E_\rho\,\epsilon_{\rho\rho} + \nu_\rho\,E_\theta\,\epsilon_{\theta\theta})\,,$$
$$\sigma_{\theta\,\theta} = \frac{1}{1-\nu_\rho\nu_\theta}(\nu_\theta\,E_\rho\,\epsilon_{\rho\rho} + E_\theta\,\epsilon_{\theta\theta})\,, \qquad \sigma_{\rho\,\theta} = 2\,G\,\epsilon_{\rho\theta}\,, \tag{17}$$

where $E_\rho, E_\theta, \nu_\rho, \nu_\theta$, and G are elastic constants that satisfy the inequalities

$$\frac{\nu_\rho}{E_\rho} = \frac{\nu_\theta}{E_\theta}\,, \quad E_\rho > 0\,, \quad E_\theta > 0\,, \quad G > 0, \quad (1-\nu_\rho\,\nu_\theta) > 0\,. \tag{18}$$

Since uniqueness is guaranteed in classical linear elasticity, the displacement field must be rotationally symmetric with respect to the center of the disk, i.e., $\mathbf{u}(\rho,\theta) = u(\rho)\,\mathbf{e}_\rho$. Thus, the strain components take the form

$$\epsilon_{\rho\rho} = u'\,, \qquad \epsilon_{\theta\theta} = \frac{u}{\rho}\,, \qquad \epsilon_{\rho\theta} = 0\,, \tag{19}$$

where $(\cdot)' \equiv d\,(\cdot)/d\,\rho$. Also, there is only one non-trivial equilibrium equation, which is given by $\partial\sigma_{\rho\rho}/\partial\rho + (\sigma_{\rho\rho} - \sigma_{\theta\theta})\,/\rho = 0$. Because of (16)-(19), this equation becomes $E_\rho\,\left(u'' + \frac{u'}{\rho}\right) - E_\theta\,\frac{u}{\rho^2} = 0$.

Imposing the natural compatibility condition $u(0) = 0$ and the boundary condition $\sigma_{\rho\rho}(\rho_e) = -p$, we obtain the *classical solution* presented in [3],

$$u(\rho) = -q\,\frac{\rho^k}{\rho_e^{k-1}}\,, \qquad q \equiv \frac{p\,(1-\nu_\rho\,\nu_\theta)}{\sqrt{E_\rho\,E_\theta} + \nu_\rho\,E_\theta}\,, \qquad \kappa \equiv \sqrt{\frac{E_\theta}{E_\rho}} > 0\,. \tag{20}$$

As remarked by Lekhnitskii, a consequence of both (20.a,c) is that the radial and tangential stresses become singular for any $p > 0$ when $\kappa < 1$, since

$$\sigma_{\rho\rho} = -p\left(\frac{\rho}{\rho_e}\right)^{k-1}\,, \quad \sigma_{\theta\theta} = -p\,\kappa\left(\frac{\rho}{\rho_e}\right)^{k-1}\,. \tag{21}$$

Another interesting feature of the solution (20.a,c), noted by [4], is that for any $p > 0$ there is a core region defined by

$$0 < \left(\frac{\rho}{\rho_e}\right)^{1-\kappa} < q \tag{22}$$

for which $u(\rho) < -\rho$. Since the deformation of the body is given by $\mathbf{f}(\mathbf{x}) = [\rho + u(\rho)]\,\mathbf{e}_\rho$ for each particle $\mathbf{x} = (\rho,\theta)$ of the disk, we readily see that material penetrates itself in this central core.

Mechanics of Solids in Brazil 2007, Marcílio Alves & H.S. da Costa Mattos (Editors)
Brazilian Society of Mechanical Sciences and Engineering, ISBN 978-85-85769-30-7

This core contains an annular region, defined by $\kappa\, q < \left(\frac{\rho}{\rho_e}\right)^{1-\kappa} < q$, where the determinant of the deformation gradient, given by

$$\det \nabla \mathbf{f} = \left[1 - \kappa\, q \left(\frac{\rho}{\rho_e}\right)^{\kappa-1}\right] \left[1 - q \left(\frac{\rho}{\rho_e}\right)^{\kappa-1}\right], \tag{23}$$

is negative. Outside the annular region, i.e., for small and large values of $(\rho/\rho_e)^{1-\kappa}$, we see from (23) that $\det \nabla \mathbf{f}$ is positive.

Thus, for $0 < \kappa < 1$, the classical solution has no physical meaning and therefore should be rejected as a viable solution. The anomalous behavior of material overlapping provides, however, motivation to use a pseudo-linear theory which respects the constraint that admissible deformations be at least locally invertible, i.e., that $\det \nabla \mathbf{f} > 0$.

3.2 The constrained Lekhnitskii problem

Reference [4] consider the solution of the rotationally symmetric disk problem of Lekhnitskii outlined in Section 3.1 for the material parameter $\kappa \in (0, 1)$ of (20.c) within the constrained minimization theory outlined in Section 2.

The sets $\mathcal{B}_=$ and $\mathcal{B}_>$ of (5), where the constraint of local injectivity is active ($\det \nabla \mathbf{f} = \varepsilon$) and non-active ($\det \nabla \mathbf{f} > \varepsilon$), respectively, can be determined explicitly as

$$\mathcal{B}_= = \{\mathbf{x} = \rho\, \mathbf{e}_\rho \in \mathcal{B} : 0 \le \rho < \rho_a\}], \qquad \mathcal{B}_> = \{\mathbf{x} = \rho\, \mathbf{e}_\rho \in \mathcal{B} : \rho_a < \rho < \rho_e\}, \tag{24}$$

for some $\rho_a \in [0, \rho_e]$, which is the solution of the algebraic equation

$$\begin{aligned} 0 = &\left(\frac{1+\kappa}{1-\nu_\rho\, \nu_\theta}\right) (E_\rho\, \kappa + \nu_\rho\, E_\theta) \left(\frac{\rho_e}{\rho_a}\right)^{\kappa-1} + \\ &\left(\frac{1-\kappa}{1-\nu_\rho\, \nu_\theta}\right) (E_\rho\, \kappa - \nu_\rho\, E_\theta) \left(\frac{\rho_e}{\rho_a}\right)^{\kappa-1} + \frac{2\,\kappa\, p}{\sqrt{\varepsilon} - 1}, \end{aligned} \tag{25}$$

with κ defined by (20.c).

The equations (6)-(8) can be solved in closed form, yielding the Lagrange multiplier constraint stress field $\lambda(\rho) = -\left(\frac{1-\sqrt{\varepsilon}}{\sqrt{\varepsilon}}\right)\left(\frac{E_\rho - E_\theta}{1-\nu_\rho\, \nu_\theta}\right) \log\left(\frac{\rho}{\rho_a}\right)$ in $\mathcal{B}_=$. Note that λ has a logarithmic singularity at the origin, which is weaker than the stress singularity of the unconstrained problem reported in (21).

Also, the displacement field $\mathbf{u} = u(\rho)\, \mathbf{e}_\rho$ is given by

$$u(\rho) = \begin{cases} -\,(1 - \sqrt{\varepsilon})\, \rho & \text{in} \quad \mathcal{B}_=, \\ \left(\frac{1+\kappa}{2\,\kappa}\right)(\sqrt{\varepsilon} - 1)\, \rho_a^{-\kappa+1}\, \rho^{\kappa} + \left(\frac{-1+\kappa}{2\,\kappa}\right)(\sqrt{\varepsilon} - 1)\, \rho_a^{\kappa+1}\, \rho^{-\kappa} & \text{in} \quad \mathcal{B}_>. \end{cases} \tag{26}$$

Using (26) together with $\mathbf{f}(\rho) = [\rho + u(\rho)]\,\mathbf{e}_\rho$, we can easily obtain the expression

$$\det \nabla \mathbf{f}(\rho) = \begin{cases} \varepsilon & \text{in} \quad \mathcal{B}_= \,, \\ \left\{1 + \frac{\sqrt{\varepsilon}-1}{2\,\kappa}\left[(\kappa+1)\left(\frac{\rho}{\rho_a}\right)^{\kappa-1} + (\kappa-1)\left(\frac{\rho}{\rho_a}\right)^{-\kappa-1}\right]\right\} * & \\ \quad \left\{1 + \frac{\sqrt{\varepsilon}-1}{2}\left[(\kappa+1)\left(\frac{\rho}{\rho_a}\right)^{\kappa-1} - (\kappa-1)\left(\frac{\rho}{\rho_a}\right)^{-\kappa-1}\right]\right\} & \text{in} \quad \mathcal{B}_> \,. \end{cases} \tag{27}$$

The solution (26) describes the deformation of the disk which is, in fact, globally injective.

4 The discrete formulation

We want to construct an approximate solution to both minimization problems (11) and (15) for given penalty parameters γ and δ, respectively. For this, we consider a Finite Element formulation based on the introduction of discrete minimization problems over a finite-dimensional space $\mathcal{A}_h \subset \mathcal{A}$, where the subscript h stands for the characteristic length of the finite element and $\mathcal{A}$ is given by (4). These problems can be solved using an unconstrained minimization method with a line search technique.

Holding h fixed and increasing γ in the interior penalty formulation, we generate a sequence of solutions parameterized by γ for the discrete problems that converges to an approximate solution $\mathbf{u}_h$ of the minimization problem (1)-(3) as $\gamma \to \infty$. We then refine the Finite Element mesh by decreasing h and repeat the process above. In so doing, we generate a sequence of solutions $\mathbf{u}_h$ parameterized by h which converges to the solution $\mathbf{u}$ of the original minimization problem (1)-(3).

A similar procedure is used to generate a convergent sequence of solutions $\mathbf{u}_h$ for the exterior penalty formulation. Here, however, $\mathbf{u}_h$ is the limit function of a sequence of solutions parameterized by δ as δ tends to zero.

The procedures outlined above are general an apply to problems in any dimension. In this work, we consider the model problem of Lekhnitskii described in Section 3 with the imposition of the injectivity constraint $\det(\mathbf{1} + \nabla \mathbf{v}) \geq \varepsilon > 0$, where $\mathbf{v} \in \mathcal{A}$. Although the problem is two-dimensional, we recall from Section 3 that it is also rotationally symmetric, so that $\mathbf{v} = v\,\mathbf{e}_\rho$, where v is a scalar function defined on the interval $(0, \rho_e)$.

Since the energy potential $\mathcal{E}[\cdot]$ is given by (1.b) and (2), we can write

$$\mathcal{E}[v\,\mathbf{e}_\rho] = \frac{\pi\,E_\rho}{1-\nu_\rho\,\nu_\theta}\left\{\int_0^{\rho_e}\left[(v')^2\,\rho + \frac{(\kappa\,v)^2}{\rho}\right]\,d\rho + \nu_\rho\,[\kappa\,v(\rho_e)]^2\right\} + 2\,\pi\,p\,v(\rho_e)\,\rho_e \tag{28}$$

for the model problem of Lekhnitskii, where κ is given by (20.c). Since $\det(\mathbf{1}+\nabla(v\,\mathbf{e}_\rho)) = (1+v')(1+v/\rho)$, the inverse barrier functional, defined by (10), becomes

$$\mathcal{Q}[v\,\mathbf{e}_\rho] = 2\,\pi \int_0^{\rho_e} \frac{\rho}{(1+v')(1+v/\rho)-\varepsilon}\,d\rho\,, \tag{29}$$

and the exterior penalty functional, defined by (13) and (14), becomes

$$\mathcal{P}[v\,\mathbf{e}_\rho] = \frac{\pi}{4} \int_0^{\rho_e} \left[-(1+v')(1+v/\rho)+\varepsilon+|(1+v')(1+v/\rho)-\varepsilon|\right]^2\,\rho\,d\rho\,. \tag{30}$$

The penalized potential $\mathcal{E}_\gamma[\cdot]$ is then obtained from (9), (28), and (29), while the penalized potential $\mathcal{E}_\delta[\cdot]$ is obtained from (12), (28), and (30).

Now, let $0=\rho_0<\rho_1<\rho_2<\ldots<\rho_n=\rho_e$ be a partition of the interval $\mathcal{I}\equiv(0,\rho_e)$ in sub-intervals $\mathcal{I}_j=(\rho_{j-1},\rho_j)$ of length $\Delta\rho_j=\rho_j-\rho_{j-1}\,, j=1,2,\ldots,n$. Let also $\mathcal{A}_h$ be the set of functions $v\,\mathbf{e}_\rho$ such that v is linear over each sub-interval $\mathcal{I}_j$, $v\in\mathcal{C}^0(\mathcal{I})$, and $v(0)=0$. Clearly, $\mathcal{A}_h\subset\mathcal{A}$, where $\mathcal{A}$ is given by (4).

Next, introduce the piecewise linear basis functions $\phi_j\,\mathbf{e}_\rho\in\mathcal{A}_h, j=1,2,\ldots,n$, defined by $\phi_j(\rho_i)=\delta_{ij}\,, i,j=1,2,\ldots,n$. Then, a function $v_h\,\mathbf{e}_\rho\in\mathcal{A}_h$ has the representation

$$v_h(\rho) = \mathbf{s}\cdot\mathbf{g}(\rho)\,, \qquad \rho\in\mathcal{I}\,, \tag{31}$$

which is the inner product between the vector $\mathbf{s}\equiv(\eta_1,\eta_2,\ldots,\eta_n)\in\mathbb{R}^n$ and the n-dimensional vector-valued function $\mathbf{g}\equiv(\phi_1,\phi_2,\ldots,\phi_n)$ defined over the interval $\mathcal{I}$. The coefficients η_i are given by

$$\eta_i = v_h(\rho_i)\,. \tag{32}$$

Substituting v_h into (28)-(30), we obtain

$$\mathcal{E}_h(\mathbf{s}) \equiv \frac{\mathcal{E}[(\mathbf{s}\cdot\mathbf{g})\,\mathbf{e}_\rho]}{2\,\pi\,p\,\rho_e} = \frac{E_\rho}{2\,(1-\nu_\rho\,\nu_\theta)\,p\,\rho_e}\left\{\int_0^{\rho_e}\left[(\mathbf{s}\cdot\mathbf{g}')^2\,\rho+\frac{(\kappa\,\mathbf{s}\cdot\mathbf{g})^2}{\rho}\right]d\rho+\right.$$

$$\left.\nu_\rho\,[\kappa\,\mathbf{s}\cdot\mathbf{g}(\rho_e)]^2\right\}+\mathbf{s}\cdot\mathbf{g}(\rho_e)\,, \tag{33}$$

$$\mathcal{Q}_h(\mathbf{s}) \equiv \frac{\mathcal{Q}[(\mathbf{s}\cdot\mathbf{g})\,\mathbf{e}_\rho]}{2\,\pi\,p\,\rho_e} = \frac{1}{p\,\rho_e}\int_0^{\rho_e}\frac{\rho}{[(1+\mathbf{s}\cdot\mathbf{g}')(1+\mathbf{s}\cdot\mathbf{g}/\rho)-\varepsilon]}\,d\rho\,, \tag{34}$$

$$\mathcal{P}_h(\mathbf{s}) \equiv \frac{\mathcal{P}[(\mathbf{s}\cdot\mathbf{g})\,\mathbf{e}_\rho]}{2\,\pi\,p\,\rho_e} = \frac{1}{8\,p\,\rho_e}\int_0^{\rho_e}\Big[-(1+\mathbf{s}\cdot\mathbf{g}')(1+\mathbf{s}\cdot\mathbf{g}/\rho)+\varepsilon+$$

$$|(1+\mathbf{s}\cdot\mathbf{g}')(1+\mathbf{s}\cdot\mathbf{g}/\rho)-\varepsilon|\Big]^2\,\rho\,d\rho\,, \tag{35}$$

respectively. Observe from (31)-(35) that $\mathcal{E}_h$, $\mathcal{Q}_h$, and $\mathcal{P}_h$ are scalar functions of an n-dimensional vector of coefficients $\eta_i, i = 1, 2, \ldots, n$. Also, $\mathcal{P}_h$ is a continuous function of $\mathbf{s}$ with continuous first derivative.

The discrete versions of the penalized potentials $\mathcal{E}_\gamma[\cdot]$ and $\mathcal{E}_\delta[\cdot]$ are then defined by

$$\mathcal{F}_\gamma(\mathbf{s}) \equiv \mathcal{E}_h(\mathbf{s}) + \frac{1}{\gamma}\mathcal{Q}_h(\mathbf{s}), \qquad\qquad \mathcal{F}_\delta(\mathbf{s}) \equiv \mathcal{E}_h(\mathbf{s}) + \frac{1}{\delta}\mathcal{P}_h(\mathbf{s}), \tag{36}$$

respectively, for a fixed h. The discrete version of the minimization problem (11), applied to the constrained disk problem of Section 3.2, consists of finding an n-dimensional vector $\mathbf{r}_\gamma \equiv \{\chi_1, \chi_2, \ldots, \chi_n\}$ that minimizes the scalar function $\mathcal{F}_\gamma$, given by (36.a), over all vectors $\mathbf{s}$ in $\mathbb{R}^n$. A similar statement is also true for the discrete version of the minimization problem (15).

The discrete minimization problems stated above are solved iteratively using a standard unconstrained second-order minimization method with a line search technique. The method is based on an *iterative descent algorithm* described in [6]. Below, we describe briefly the algorithm for the minimization problem

$$\min_{\mathbf{s}\in\mathbb{R}^n} \mathcal{F}_\gamma(\mathbf{s})\,, \tag{37}$$

where $\mathcal{F}_\gamma$ is given by (36.a) together with (33) and (34).

Starting from an initial guess $\mathbf{s}_0 \in \mathbb{R}^n$, which corresponds to the undistorted natural state of the body, and from a known direction of steepest descent $\mathbf{d}_0$, we generate a sequence of approximate solutions $\mathbf{s}_k, k = 0, 1, 2, \ldots$, denoted by $\{\mathbf{s}_k\} \in \mathbb{R}^n$, using the recursive formula $\mathbf{s}_{k+1} = \mathbf{s}_k + \alpha_k\,\mathbf{d}_k$, where α_k is a scalar minimizing $\mathcal{F}_\gamma$ in a given direction of search $\mathbf{d}_k$. The sequence of points $\{\mathbf{s}_k\}$ converges to the solution $\mathbf{r}_\gamma \in \mathbb{R}^n$ of the discrete minimization problem (37).

Next, we increase the penalty parameter γ and repeat the whole minimization process outlined above. Now, however, we start the new minimization process taking for $\mathbf{s}_0$ the limit point $\mathbf{r}_\gamma$ of the previous minimization process. The initial direction of search $\mathbf{d}_0$ is the direction of steepest descent evaluated at the new point $\mathbf{s}_0$. Using this procedure for a fixed h, we generate a sequence $\{\mathbf{r}_\gamma\}$ that converges to a limit point $\mathbf{r}_h \in \mathbb{R}^n$ as $\gamma \to 0$. We use $\mathbf{r}_h$ together with the representation (31) to construct the function $\mathbf{u}_h = (\mathbf{r}_h \cdot \mathbf{g})\,\mathbf{e}_\rho$. This function is an approximation of the solution $\mathbf{u}$ of the original problem (1)-(3) for a fixed h. Letting $h \to 0$, we generate a sequence $\{\mathbf{u}_h\}$ that converges to $\mathbf{u}$.

The algorithm for the minimization problem

$$\min_{\mathbf{s}\in\mathbb{R}^n} \mathcal{F}_\delta(\mathbf{s})\,, \tag{38}$$

where $\mathcal{F}_\delta$ is given by (36.b) together with (33) and (35), is similar to the algorithm described above. Here, however, we let $\delta \to 0$ in order to generate a sequence $\{\mathbf{r}_\delta\}$ that converges to the limit point $\mathbf{r}_h \in \mathbb{R}^n$.

5 Numerical results

We apply the numerical method discussed in Section 4 to solve numerically the constrained disk problem described in Section 3.2. We have normalized all lengths by setting the radius of the disk $\rho_e = 1$. Furthermore, in dimensionless units, the applied load on the boundary of the disk is $p = 500$, and the elastic constants are $c_{11} \equiv E_\rho/(1-\nu_\rho\,\nu_\theta) = 10^5$, $c_{22} \equiv E_\theta/(1-\nu_\rho\,\nu_\theta) = 10^3$, $c_{12} \equiv \nu_\rho\, c_{22} = 10^3$, which, in view of (20.c), yield $\kappa = 0.1 < 1$. Also, we take $\varepsilon = 0.1$ for the lower bound of the injectivity constraint[1]. The radius of the core subregion $\mathcal{B}_=$ where the constraint is active is calculated from (25), yielding $\rho_a \cong 0.00583$. In addition, we use uniform partitions of the interval $(0, \rho_e)$ to simulate a case for which the active region $\mathcal{B}_=$ is both not empty and unknown. The most refined mesh in this work has 4096 elements.

In Fig. 1 we show two graphs with both the exact analytical solution, given by (26) and represented by the solid line, and the numerical solutions, obtained with the regular mesh of 4096 elements and represented by the dash-dotted lines. The graph on the left side was obtained with the interior penalty formulation using increasing values of γ and the graph on the right side was obtained with the exterior penalty formulation using decreasing values of δ. We see from both graphs that the sequences of numerical solutions converge to limit functions that can not be distinguished from the analytical solution. Observe from the graph on the left side that the displacement field for $\gamma = 1$ is positive in $(0, \rho_e)$, even though the disk is under compression. This numerical solution has no physical meaning and it only provides a starting point in the search procedure for the next solution in the sequence of solutions parameterized by γ, (see Section 5).

In Fig. 2 we show curves for the base 10 logarithm of the error between the exact solution $\mathbf{u} = u\,\mathbf{e}_\rho$, given by (26), and the numerical solution $\mathbf{u}_h = (\mathbf{r}_h \cdot \mathbf{g})\,\mathbf{e}_\rho$, using the regular mesh of 4096 elements. This error is plotted against both the base 10 logarithm of the parameter γ of the interior penalty formulation in the graph on the left side and the base 10 logarithm of the parameter $1/\delta$ of the exterior penalty formulation in the graph on the right side. For both formulations, the solid line represents the energy norm of the error, which is defined by $\|\mathbf{u}-\mathbf{u}_h\|_E = \mathcal{F}(u-u_h)$, where $\mathcal{F}$ is given by either (36.a) together with (33) and (34) for the interior penalty formulation or (36.b) together with (33) and (35) for the exterior penalty formulation. The dash-dotted line represents the Euclidean norm of the error, $\|\mathbf{r} - \mathbf{r}_h\|_2$, for both formulations, where the components of $\mathbf{r}$ are given by $\xi_i = u(\rho_i)$, $i = 1, 2, \ldots, n$. Observe in the graph on the left side that $\|\mathbf{r}-\mathbf{r}_h\|_2$ decreases monotonically with increasing values of γ and tends to an assymptotic value as γ becomes large. A similar behavior is observed for $\|\mathbf{u}-\mathbf{u}_h\|_E$, except that there is a point off the curve for $\gamma = 10^5$. For the graph on the right side, observe that both errors are almost constant for small and large values of δ and that they decrease rapidly in an

[1] These geometric and material constants are used by [4] and [5] in their analytical and numerical analyses, respectively, of the compressed disk problem.

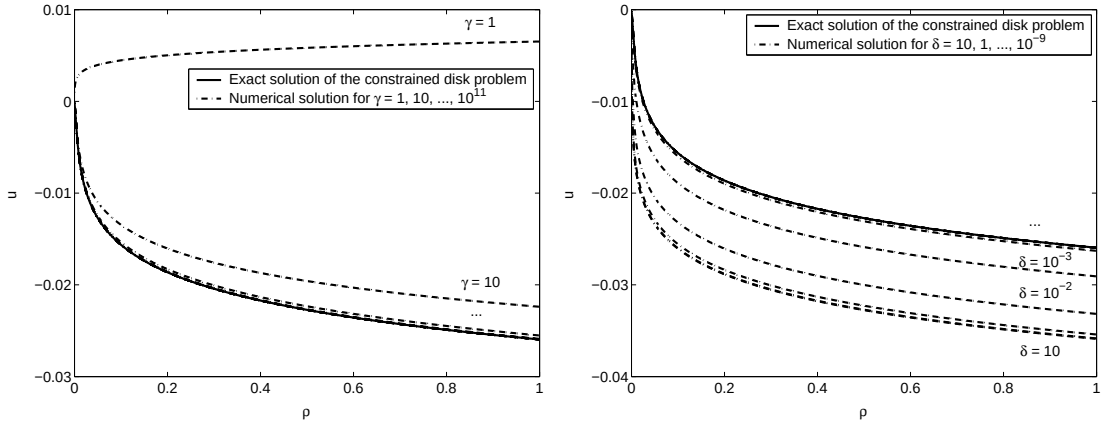

Figure 1: Radial displacement u versus radius ρ for the constrained disk problem with a fixed h.

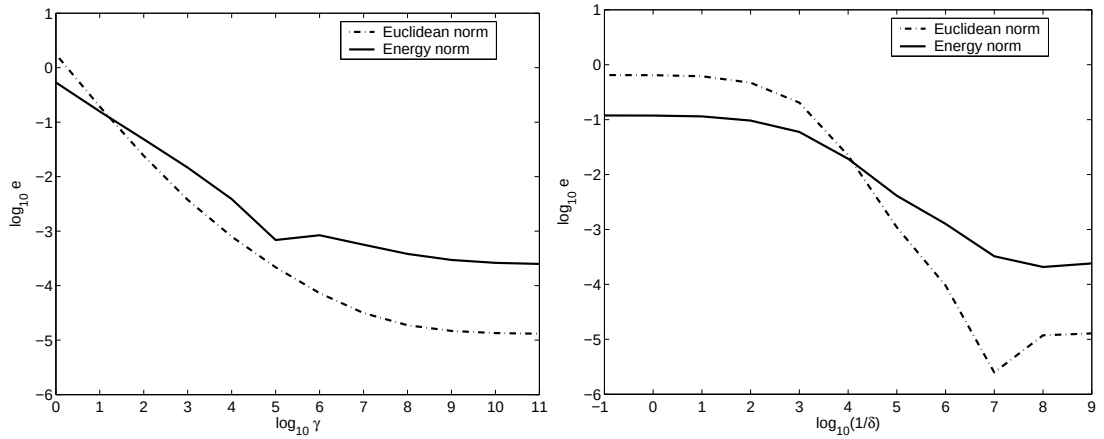

Figure 2: Base 10 logarithm of the error e versus base 10 logarithm of the parameter a) γ (left), b) $1/\delta$ (right). Solid line: $e \equiv \|\mathbf{u}_h - \mathbf{u}\|_E$. Dash-dotted line: $e \equiv \|\mathbf{r} - \mathbf{r}_h\|_2$.

interval of intermediate values of δ. Notice a point off the curve for $\|\mathbf{r} - \mathbf{r}_h\|_2$ when $\delta = 10^{-7}$.

In both graphs shown in Fig. 2 we see that the errors tend to assymptotic values as both γ and $1/\delta$ tend to infinity. In Fig. 3 we show curves for the base 10 logarithm of the Euclidean error $\|\mathbf{r}_b - \mathbf{r}_h\|_2$ between the best numerical solution $u_b \equiv \mathbf{r}_b \cdot \mathbf{g}$, obtained with large values of either γ or $1/\delta$ for each discretization, and the numerical solution $u_h = \mathbf{r}_h \cdot \mathbf{g}$. This error is plotted against both the base 10

logarithm of the parameter γ in the graph on the left side and the base 10 logarithm of the parameter $1/\delta$ in the graph on the right side.

Observing the graph on the left side of Fig. 3, we see that $\|\mathbf{r}_b - \mathbf{r}_h\|_2$ decreases monotonically with increasing values of γ and that, except for the curve obtained with 256 elements, which is represented by the plus sign, all the other curves are similar to each other. In particular, notice that all these curves are almost straight lines for $\gamma > 10^4$. Performing a linear regression on the curve corresponding to 4096 elements, which is represented by the solid line, we find that the angular coefficient is approximately equal to -0.54, which corresponds to a convergence ratio of $10^{-0.54} \cong 0.29$[2]. Similar analyses can be performed on the curves shown in the graph on the right side of Fig. 3. In this case, all but the curve corresponding to 256 elements, are almost straight lines for $1/\delta > 10^5$. In this case, the angular coefficient obtained from a linear regression analysis of the curve corresponding to 4096 elements is approximately equal to -1.02, which corresponds to a convergence ratio of $10^{-1.02} \cong 0.096$.

We see from the exposition above that, for a sufficiently large value of n, the sequence of numerical solutions parameterized by δ converges faster to a limit function than the sequence of numerical solutions parameterized by γ. On the other hand, this convergence is more uniform for the sequence of solutions parameterized by γ than it is for the sequence of solutions parameterized by δ. In particular, notice that this last sequence yields a convergence ratio close to one for large values of δ. To see this, we performed a linear regression analysis on the curve corresponding to 4096 elements for $1/\delta < 10$ and found that the angular coefficient is approximately equal to -0.01.

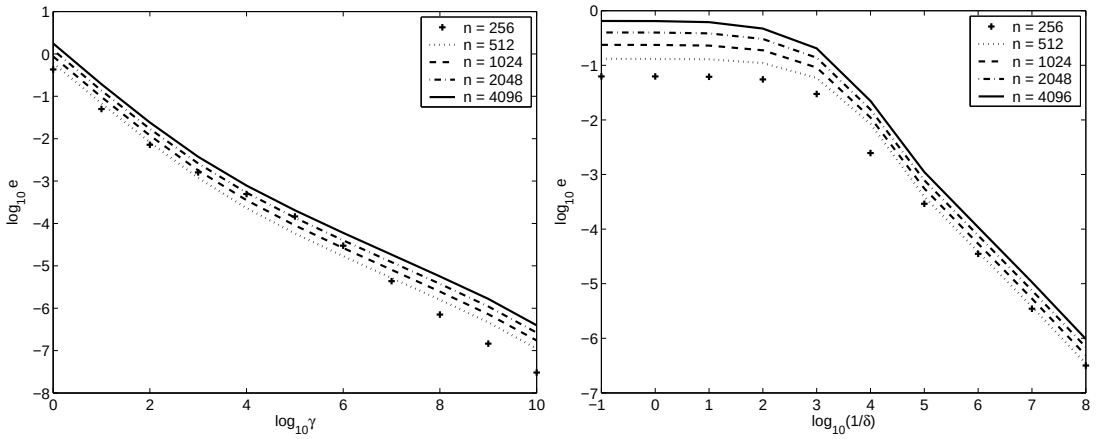

Figure 3: Base 10 logarithm of the Euclidean error $e = \|\mathbf{r}_b - \mathbf{r}_h\|_2$ versus base 10 logarithm of the parameter a) γ (left), b) $1/\delta$ (right).

[2]Consider the ratio between two consecutive values of a sequence of real numbers. If this ratio tends to a constant value as the number of terms in the sequence tends to infinity, then the ratio is called the convergence ratio of the sequence.

Next, we chose the largest value of either γ or $1/\delta$ for each discretization and obtained curves for both the exact analytical solution, given by (26), and the corresponding numerical solution. These curves are shown in Fig. 4. The analytical solution is represented by the solid line and the numerical solutions are represented by the dash-dotted lines. The graph shown in the figure is identical to the graph obtained with either the interior penalty formulation with a fixed large γ or the exterior penalty formulation with a fixed small δ. Observe that the numerical solution converges to the analytical solution as $h \equiv \rho_e/n \to 0$, where n is the number of elements. In addition, a numerical solution obtained from a coarse mesh, with only 64 elements, is already a good approximation for the exact solution in both cases, even though the distance of the nearest node to the origin, given by $\rho_1 \equiv h = 0.015625$ for a regular mesh, is greater than the radius of $\mathcal{B}_=$, given by $\rho_a \cong 0.00583$.

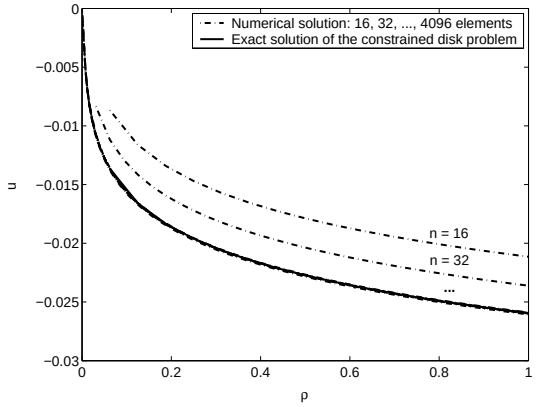

Figure 4: Radial displacement u versus radius ρ for the constrained disk problem for either large γ or small δ.

In Fig. 5 we show curves for the base 2 logarithm of the error between the exact solution $\mathbf{u} = u\,\mathbf{e}_\rho$, given by (26), and the numerical solution $\mathbf{u}_h = (\mathbf{r}_h \cdot \mathbf{g})\,\mathbf{e}_\rho$ versus the base 2 logarithm of the number of elements n. The solid line represents the energy norm of the error, $\|\mathbf{u} - \mathbf{u}_h\|_E$, and the dash-dotted line represents the Euclidean norm of the error, $\|\mathbf{r} - \mathbf{r}_h\|_2$, where we recall from above that the components of $\mathbf{r}$ are given by $\xi_i = u(\rho_i)$, $i = 1, 2, \ldots, n$. Results for the interior and exterior formulations are shown in the left and right graphs, respectively. Observe that the graphs are very similar to each other. In both cases the error decreases with the increasing number of elements up to 128 elements, which corresponds to the distance $\rho_1 = 0.00781$, then increases and reaches a peak for $n = 256$, which corresponds to $\rho_1 = 0.00391$, decreasing thereafter. These two values of ρ_1 are, respectively, above and below the value of $\rho_a \cong 0.00583$.

Notice from Fig. 5 that all curves are almost straight lines for $n \geq 1024$ elements. Performing a linear regression on these curves, we found that, for both formulations, the angular coefficient is

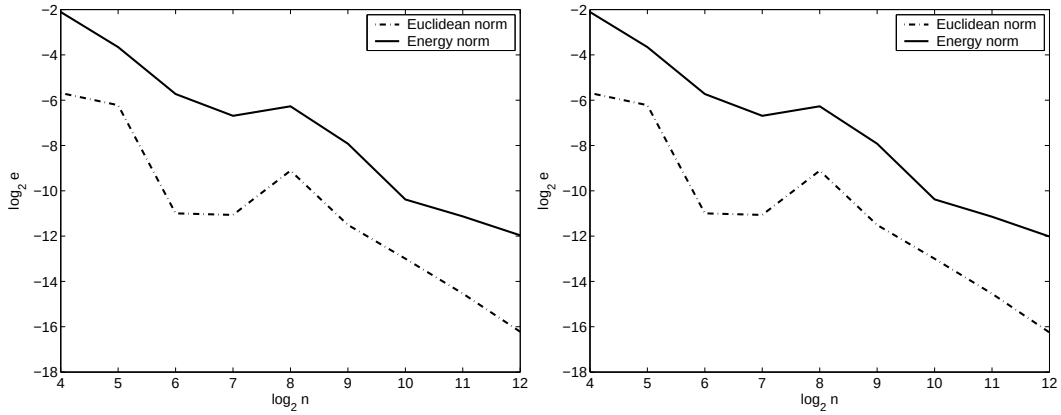

Figure 5: Base 2 logarithm of the error e versus base 2 logarithm of the number of elements n. Left: Interior penalty formulation with large γ. Right: Exterior penalty formulation with small δ. Solid line: $e \equiv \|u_h - u\|_E$. Dash-dotted line: $e \equiv \|u_h - u\|_2$.

approximately equal to -0.8 for the energy norm of the error and to -1.6 for the Euclidean norm of the error. These values correspond to convergence ratios of $2^{-0.8} \cong 0.57$ and of $2^{-1.6} \cong 0.34$, respectively.

6 Conclusion

We presented a comparative study between an interior and an exterior penalty formulation for a class of constrained minimization problems considered by [4]. A constrained problem in this class consists of finding a minimizer $\mathbf{u}$ for the total potential energy $\mathcal{E}$ of classical linear theory of elasticity over a set $\mathcal{A}_\varepsilon$ of admissible displacement fields that satisfy the local injectivity constraint $\det(\mathbf{1}+\nabla\mathbf{u})-\varepsilon \geq 0$ for a sufficiently small $\varepsilon \in \mathbb{R}$.

In Section 5 we showed numerical results that are in very good agreement with analytical results presented in Section 3.2. In addition, we showed some convergence results which indicate that, for a fixed characteristic length h of the finite element mesh, the sequence of numerical solutions obtained with the exterior penalty formulation converges faster to a limit function than the sequence of numerical solutions obtained with the interior penalty formulation. The results also indicate that this limit function is the same for both formulations. We then constructed a sequence of limit functions u_h and observed that the convergence ratio for this sequence is the same for either one of the formulations, even though the convergence ratio obtained with the energy norm of the error is significantly different from the Euclidean norm of the error.

Acknowledgements

The author wishes to acknowledge FAPESP (Fundação de Amparo a Pesquisa do Estado de São Paulo), proc. # 2005/00409-0 for its support of this research.

References

[1] Aguiar, A.R., A numerical treatment of material overlapping in elasticity. *Iberian Latin American Congress on Computational Methods in Engineering (XXV CILAMCE)*, 2004.
[2] Aguiar, A.R., An exterior penalty method to prevent material overlapping in elasticity. *Iberian Latin American Congress on Computational Methods in Engineering (XXVII CILAMCE)*, 2006.
[3] Lekhnitskii, S.G., *Anisotropic Plates*. New York: Gordon and Breach Science Publishers, 1968.
[4] Fosdick, R.L. & Royer, G., The constraint of local injectivity in linear elasticity theory. *Proc R Soc Lond A*, **457**, pp. 2167–2187, 2001.
[5] Obeidat, K., Stolarski, H., Fosdick, R. & Royer-Carfagni, G., Numerical analysis of elastic problems with injectivity constraints. *European Conference on Computational Mechanics (ECCM-2001)*, 2001.
[6] Aguiar, A.R., Local and global injective solution of the rotationally symmetric sphere problem. *Journal of Elasticity*, **84**, pp. 99–129, 2006.